Dalton Transactions

Accepted Manuscript

ROYAL SOCIETY OF CHEMISTRY

www.rsc.org/dalton

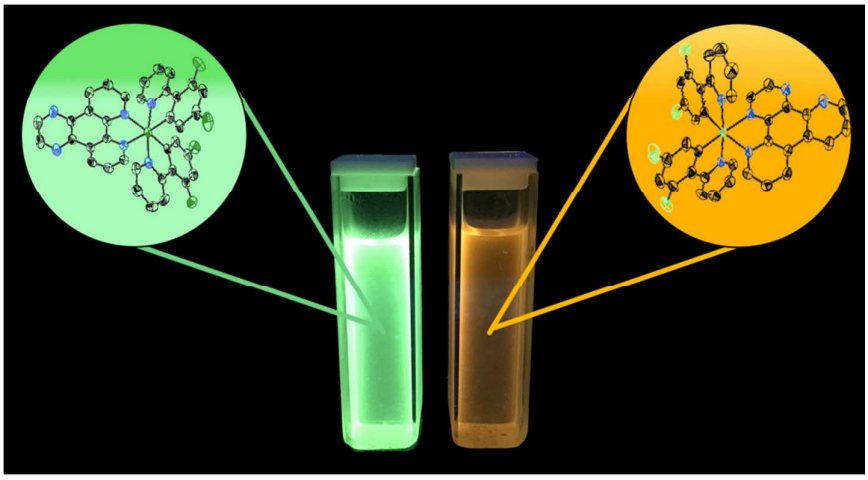

Two new cationic Ir(III) complexes are compared with respect to their performance in light electrochemical cells (LECs).

Cite this: DOI: 10.1039/c0xx00000x

www.rsc.org/xxxxxx

ARTICLE TYPE

Comparative study of Ir(III) complexes with pyrazino[2,3-f][1,10]phenanthroline and pyrazino[2,3-f][4,7]phenanthroline ligands in light-emitting electrochemical cells (LECs)

Iván González,[a] Paulina Dreyse,[b] Diego Cortés-Arriagada,[c] Mahesh Sundararajan,[d] Claudio Morgado,[b] Iván Brito,[e] Cristina Roldán-Carmona,[f] Henk J. Bolink,*[f] and Bárbara Loeb*[a]

Received (in XXX, XXX) XthXXXXXXXXX 20XX, Accepted Xth XXXXXXXXX 20XX
DOI: 10.1039/b000000x

We report the comparative study of the electrochemical and photoluminescent properties of two Ir(III) complexes described as $[Ir(F_2ppy)_2(N^N)][PF_6]$, where the F_2ppy ligand is 2-(2,4-difluorophenyl)pyridine and the N^N ligands are pyrazino[2,3-f][1,10]phenanthroline (ppl) and pyrazino[2,3-f][4,7]phenanthroline (ppz). The complexes were used for the fabrication of light-emitting electrochemical cells (LECs). The structures of the complexes have been corroborated by X-ray crystallography. Theoretical calculations were performed to understand the photophysical behavior of the complexes. Both in solution and solid state, the photoluminescent spectra shows that emission is significantly red-shifted in the $[Ir(F_2ppy)_2(ppz)][PF_6]$ complex compared with the $[Ir(F_2ppy)_2(ppl)][PF_6]$ complex. Besides, the $[Ir(F_2ppy)_2(ppl)][PF_6]$ complex exhibits a higher quantum yield and a longer excited state lifetime than the $[Ir(F_2ppy)_2(ppz)][PF_6]$ complex; therefore, in the last case non-radiative decay is predominant due to the stabilization of LUMO orbital (energy gap law). In the fabrication of LEC devices with the $[Ir(F_2ppy)_2(ppl)][PF_6]$ complex, light emission was obtained with a maximum value of luminance equal to 177 cdm^{-2}, while in the case of the $[Ir(F_2ppy)_2(ppz)][PF_6]$ complex, no luminance was observed. According to the photophysical data, the performance in LEC devices could be explained by the different position of the nitrogens in the ppl and ppz structural isomers, electronically affecting the complex, and therefore its properties. In addition, from the crystallographic analysis it is possible to note that the $[Ir(F_2ppy)_2(ppz)][PF_6]$ complex shows enhanced intermolecular and intramolecular interactions compared with $[Ir(F_2ppy)_2(ppl)][PF_6]$, and consequently it can be expected a higher ordering of the molecules in the complex with ppz ligand. This higher order could favour quenching processes, and consequently enhancing the non-radiative deactivation.

Introduction

Cyclometalated Ir(III) complexes have been widely studied due to their interesting photophysical properties and technological applications as in dye sensitized solar cells (DSSCs),[1,2] non-linear optical (NLO) devices,[3] organic light-emitting diodes (OLEDs),[4,5] and light-emitting electrochemical cells (LECs).[5-8] In particular, LECs are manufactured with a single layer of an ionic transition metal complex (iTMC), sandwiched between two electrodes, which promotes the electronic injection, the charge transport and the light emission. Unlike OLEDs, that rely on a multilayer architecture to fulfilling these functions, LECs consist of only one active layer.[9,10] In addition, the LEC devices work with air-stable cathodes, therefore, rigorous encapsulation is not necessary.[11-13] Cyclometalated Ir(III) complexes are known to experience strong spin–orbit coupling processes that allow to populate spin-forbidden triplet excited states, which are mixed with the higher ^{1}MLCT (metal-to-ligand charge transfer) state, obtaining high emission quantum yields.[5] This feature has an important influence in the high chemical and physical stability of these type of Ir-iTMCs. Consequently, they can be considered as excellent candidates for development of LEC technology.[5,14,15]

On the other hand, the emission wavelength of cationic Ir(III) complexes is affected significantly by the nature of the organic ligand. The cyclometalating and ancillary ligands in complexes of the type $[Ir(C^N)_2(N^N)]^+$ (C^N: cyclometalating ligand and N^N: substituted 2,2´-bipyridine ancillary ligand), act independently in order to achieve the desired emitting colour.[4,5] In general, electron-withdrawing substituents in the C^N ligand decrease the electronic density of the metal, producing the stabilization of the HOMO (highest occupied molecular orbital). This effect has been achieved for example by incorporation of fluorine substituents.[16,17] Alternatively, the N^N ligand can be modified with the purpose of stabilizing or destabilizing mainly the LUMO (lowest unoccupied molecular orbital), changing the HOMO–LUMO gap and therefore the emission energy.[5]

In this paper two isomers of cyclometalated Ir(III) complexes were compared in terms of their photophysical properties and

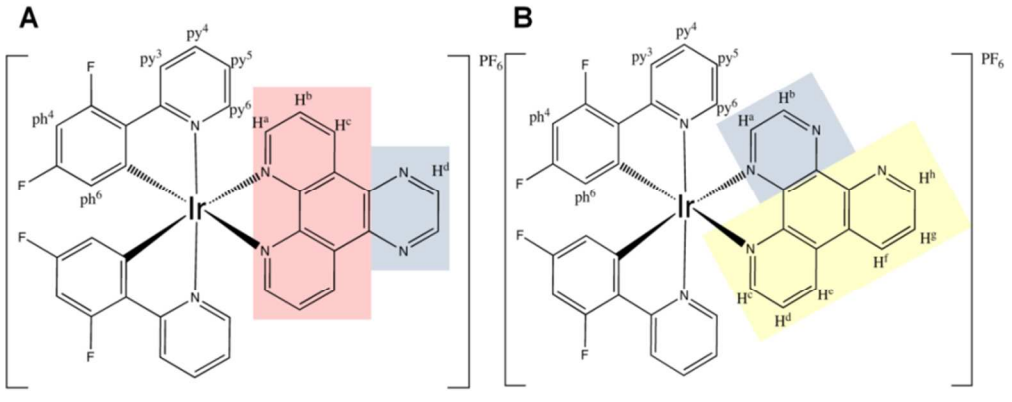

Fig. 1 Chemical structures of the cyclometalated Ir(III) complexes studied. $[Ir(F_2ppy)_2(ppl)][PF_6]$ (A) and $[Ir(F_2ppy)_2(ppz)][PF_6]$ (B). Red area: 1,10-phenanthroline, yellow area: 4,7-phenanthroline and blue area: pyrazine.

and performance in LEC devices. The studied complexes (see Figure 1) have the general formula $[Ir(F_2ppy)_2(N^N)][PF_6]$, where F_2ppy: 2-(2,4-difluorophenyl)pyridine and N^N is either pyrazino[2,3-f][1,10]phenanthroline (ppl) or pyrazino[2,3-f][4,7]phenanthroline (ppz). In conjunction with the experiments, quantum chemical calculations were carried out to understand the influence of the ancillary ligands in the electronic properties of the two Ir(III) complexes. The energy gap between the HOMO and the LUMO was analyzed, due to influence of the position of phenanthrolinic nitrogens in the structure of the N^N ligand, which determines the coordination sites of the ligand. Moreover, the performance of these complexes in LECs was evaluated. The device based on the $[Ir(F_2ppy)_2(ppl)][PF_6]$ complex showed electroluminescence, while for the devices using the $[Ir(F_2ppy)_2(ppz)][PF_6]$ complex no light emission was observed. In accordance with the experimental and theoretical studies, the different performance in LEC device is attributed to a synergistic effect between of the electron-withdrawing character of the ppz ligand and the greater number of molecular interactions observed for the complex with this ligand from X-ray crystallography. The very short turn on times for the $[Ir(F_2ppy)_2(ppl)][PF_6]$ based LEC, allows to propose this complex as an effective and promising luminescent material for artificial lighting applications.

Experimental

General

Reagents and solvents were purchased from Sigma–Aldrich, with the exception of $IrCl_3$ hydrate, which was purchased from Precious Metals Online, PMO Pty LTD, Australia. All reactions were carried out under nitrogen atmosphere. The 2-(2,4-difluorophenyl)pyridine ligand is commercially available from Sigma-Aldrich. The ppl and ppz ligands were synthesized according to reported procedures.[18-21] The cyclometalated Ir(III) chloro-bridge dimers $[Ir(F_2ppy)_2(\mu\text{-}Cl)]_2$ were synthesized following a synthetic route described in literature.[22,23]

Synthesis of the complexes

$[Ir(F_2ppy)_2(ppl)][PF_6]$. One equivalent of the starting bimetallic precursor $[Ir(F_2ppy)_2(\mu\text{-}Cl)]_2$) and 2.2 equivalents of ppl ligand were dissolved in 50 mL of $MeOH/CH_2Cl_2$ (3:1). The mixture was heated to reflux for 4 hours under nitrogen atmosphere in darkness. Next, the solution was cooled to room temperature and the volume of the solution was reduced by under vacuum. Then 500 mL of water was added and the mixture was filtered. To the obtained solution, 2 equivalents of KPF_6 were added, obtaining a yellow precipitate. This solid was filtered and washed with water, and then was purified by column chromatography on silica, eluting with acetone and then changed by ethanol. The product was recrystallized with CH_2Cl_2/diethyl ether diffusion. (89 mg, 0.09 mmol, 78%). Found: C, 46.00; H, 2.90; N, 9.00; $C_{36}H_{20}F_{10}IrN_6P$ requires C, 45.53; H, 2.12; N, 8.85%. UV-Vis λ/nm (ε/dm^3 mol^{-1} cm^{-1}) (CH_3CN) 257 (112415), 358 (13388), 419 (1887). IR (KBr,ν/cm^{-1}) 3086 (CH_{arom}), 1575 (CC), 1479 (CN), 842, 557 (PF_6^-). ^{1}H NMR (400 MHz, $(CD_3)_2CO$, 295 K) δ/ppm 9.81 (d, 2H, H^c), 9.36 (s, 2H, H^d), 8.71 (d, 2H, H^a), 8.40 (d, 2H, py^3), 8.28-8.25 (m, 2H, H^b), 8.01 (t, 1H, py^4), 7,88 (d, 2H, py^6), 7.06 (t, 2H, py^5), 6.82 (t, 2H, ph^4), 5.91 (d, 2H, ph^6) (see the ESI† for details).

$[Ir(F_2ppy)_2(ppz)][PF_6]$. One equivalent of the starting bimetallic precursor $[Ir(F_2ppy)_2(\mu\text{-}Cl)]_2$ was dissolved in a $MeOH/CH_2Cl_2$(1:3) mixture and added by dripping onto a solution of 3 equivalents of the ppz ligand dissolved in 50 mL of $MeOH/CH_2Cl_2$ (1:1). The mixture of reaction was heated to reflux for 2 hours under nitrogen atmosphere in darkness. After cooling to room temperature, the volume of the mixture was reduced under vacuum and then 500 mL of water was added. The mixture was filtered and 2.5 equivalents of KPF_6 were added to the solution, obtaining a yellow precipitate. This solid was filtered and washed with water, and then was purified by column chromatography on alumina, eluting with methanol. The product was recrystallized with CH_2Cl_2/diethyl ether diffusion. (44 mg, 0.046 mmol, 39%). Found: C, 44.93; H, 2.02; N, 8.66; $C_{36}H_{22}F_{10}IrN_6OP$ requires C, 45.53; H, 2.12; N, 8.85%. UV-Vis λ/nm (ε/dm^3 mol^{-1} cm^{-1}) (CH_3CN) 258 (75898), 298 sh (31404), 360 (10112), 456 (897). IR (KBr, ν/cm^{-1}) 3083 (CH_{arom}), 1576 (CC), 1479 (CN), 843, 557 (PF_6^-). ^{1}H NMR (400 MHz, $(CD_3)_2CO$, 295 K) δ/ppm 9.68 (d, 1H, H^e), 9.48 (d, 1H, H^h), 9.41 (d, 1H, H^a), 9.29 (d, 1H, H^f), 8.72-8.64 (m, 2H, H^b and H^e), 8.43-8.36 (m, 2H, py^3), 8.25 (t, 1H, H^d), 8.12 (t, 1H, H^g), 8.07-7.84 (m, 4H, py^{4}and py^6), 7.07 (d, 2H, py^5), 6.83 (dt, 2H, ph^4), 5.90 (dd, 2H, ph^6) (see the ESI† for details).

Crystallography

Suitable single crystals of the $[Ir(F_2ppy)_2(ppl)][PF_6]$ and $[Ir(F_2ppy)_2(ppz)][PF_6]$ complexes were selected by means of a

Table 1 Crystallographic data for:

	$[Ir(F_2ppy)_2(ppl)][PF_6]$	$[Ir(F_2ppy)_2(ppz)][PF_6]*2H_2O$
Formula	$C_{36}H_{20}F_{10}IrN_6P$	$C_{36}H_{24}F_{10}IrN_6O_2P$
Formula weight	949.75	985.78
T/K	173(2)	173(2)
Crystal system	Triclinic	Triclinic
λ/ Å	0.7107	0.7107
Space group	P -1	P -1
a, b, c/Å	8.5942(6)	9.4779(7)
	11.7450(8)	12.0740(10)
	18.1823(11)	15.5883(11)
α, β, γ/°	71.872(5)	92.099(6)
	85.630(5)	92.269(6)
	77.149(5)	97.083(7)
U/Å^3	1700.5(2)	1767.3(2)
Z	2	2
Dc/Mgm^{-3}	1.855	1.852
μ/ mm^{-1}	4.066	3.920
F(000)	920	960
Crystal size/mm^3	0.150 x 0.140 x 0.070	0.130 x 0.110 x 0.060
Θ range/°	3.362-25.644	3.324-25.632
Index ranges	-10 ≤ h ≤ 11	-11 ≤ h ≤ 11
	-14 ≤ k ≤ 14	-14 ≤ k ≤ 13
	-22 ≤ l ≤ 21	-18 ≤ l ≤ 18
Reflections collected	18851	17064
Independent reflections	6358	6597
R(int)	0.0724	0.0512
Refinement method	Full-matrix least-squares on F^2	Full-matrix least-squares on F^2
Data/restraints/ parameters	6358 /0 /487	6597/0 /505
Goodness-of-fit on F^2	1.040	0.947
R_1, wR_2 indices [I>2σ(I)]	R_1= 0.0291, wR_2= 0.0700	R_1= 0.0358, wR_2= 0.0664
R_1, wR_2(all data)	R_1 = 0.0328, wR_2 = 0.0716	R_1 = 0.0523, wR_2 = 0.0700
Largest diff. peak and hole/e.Å^{-3}	0.950, -1.338	1.306, -1.244
CCDC	1027525	1044762

polarization microscope, mounted on the tip of a glass fiber, and investigated on an STOE IPDS II two-circle-diffractometer using Mo Kα radiation (λ = 0.71073 Å). The intensities were corrected for absorption by an empirical correction with X-Area (Stoe&Cie, 2001).[24] The structure were solved by direct methods (SHELXS)[25] and refined by full-matrix least-squares calculations on F^2 (SHELXL-97). Anisotropic displacement parameters were refined for all non-hydrogen atoms. Crystallographic data are listed in Table 1.

Equipment and methods

^{1}H NMR spectra were obtained on a Bruker Avance 400 MHz instrument. The infrared spectra were recorded in a Bruker Vector-22 FT IR spectrometer on KBr pellets. UV–Vis spectra were recorded on a Shimadzu UV-Vis-NIR 3101 PC spectrophotometer. The cyclic voltammetric measurements were carried out using a CH Instruments potentiostat 760C, a platinum disc working electrode with an area of 0.02 cm^2, a saturated Ag/AgCl reference electrode and a platinum wire counter electrode. All measurements were made using acetonitrile solutions of 1 mM of Ir(III) complexes with 0.1 M of tetrabutylammonium hexafluorophosphate (TBA-PF_6) at a scan rate of 0.1 Vs^{-1}. Emission measurements were carried out in a Perkin Elmer spectrofluorimeter model SP 8765 at room temperature, with acetonitrile solutions of the complexes previously degassed with N_2 for approximately 20 min. The excitation wavelengths were 358 and 360 nm for $[Ir(F_2ppy)_2(ppl)][PF_6]$ and $[Ir(F_2ppy)_2(ppz)][PF_6]$ complexes, respectively. Emission quantum yields (Φ) were determined by the method described by Ishida et al.[26] using $[Ru(bpy)_3][PF_6]_2$ in CH_3CN as reference (Φ = 9.50 %). Steady-state and time-resolved fluorescence measurements were performed on a K2 multifrequency phase and modulation spectrofluorometer (ISS, Champaign, IL, USA). The instrument was equipped with Glan-Thompson polarizers. Excitation light was obtained by the modulable ISS 375 nm LED laser at frequencies between 10 and 150 MHz. The emission was measured through Schott KV-399 and WG-420 long band-pass filters. Lifetime measurements were made with the polarizers oriented in the ''magic angle'' at 54.7° condition.[27,28] In the multifrequency phase and modulation technique the intensity of the exciting light is modulated, and the phase shift and relative modulation of the emitted light are determined. Phase and modulation values were obtained as previously describe.[29,30] In all measurements, data were taken until the standard deviation of the phase and modulation measurements were, at each modulation frequency, smaller than 0.2° and 0.004°, respectively. Fluorescence spectra were obtained employing a 300 W Xe lamp and slits were set at 20 nm (excitation) and 5 nm (emission). The results were analyzed according to the Global Program (Global Unlimited software package, Laboratory for Fluorescence Dynamics, University of Illinois at Urbana-Champaign, Urbana, IL, USA).[31] The fitting function for the lifetime measurements was a discrete mode and a discrete component, fixed at 0.01 ns, in order to account for scattered light.[32]

The emission spectra and quantum yields of complexes in thin films prepared from 20 mgmL^{-1} solutions of Ir(III)-complex/ionic liquid (1-butyl-3-methylimidazolium hexafluorophosphate, BMIM-PF_6) in a 4:1 molar ratio, were measured using a Hamamatsu C9920-02 Absolute PL Quantum Yield Measurement System. The system is made up of an excitation light source consisting of a xenon lamp linked to a monochromator, an integration sphere and a multi-channel spectrometer.

Theoretical calculations

Density functional theory (DFT) calculations were performed at the B3LYP/TZVP level theory.[33,34] The SD (60, MWB) pseudopotential and def2-TZVP basis set were adopted for iridium.[35,36] All geometries are characterized as minima by performing numerical vibrational frequencies. Time dependent (TD) DFT calculations were performed to obtain the lowest 50 singlet exited states due to vertical excitation from the ground state by using the Tamm-Dancoff approximation.[37] Geometry optimization of the lowest triplet state was carried using the unrestricted Kohn-Sham (UKS) formalism. All calculations were performed in the ORCA 3.0 program.[38,39] The electronic population analysis was obtained with the NBO 6.0 program.[40]

Device preparation and characterization

The thicknesses of the films were determined using an Ambios XP-1 profilometer. Indium tin oxide (ITO)-coated glass plates

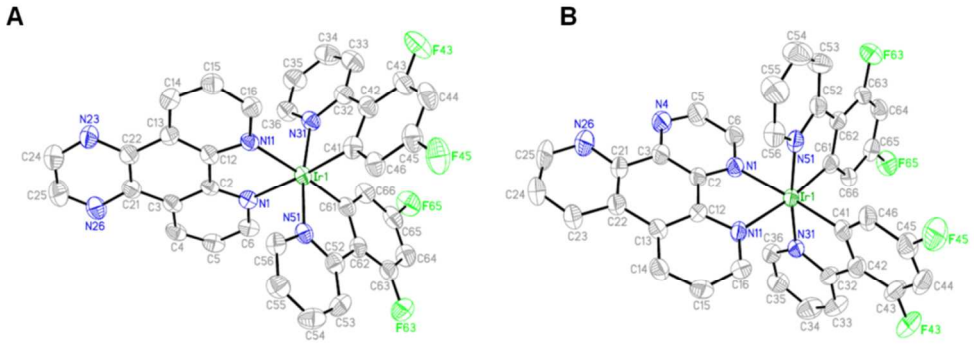

Fig. 2 Structures of $[Ir(F_2ppy)_2(ppl)]^+$ (A) and $[Ir(F_2ppy)_2(ppz)]^+$ (B). H atoms omitted.

(15 $\Omega\square^{-1}$) were patterned by conventional photolithography (www.naranjosubstrates.com). The substrates were cleaned by sonication in water-soap, water, and 2-propanol baths, in that order. After drying, the substrates were placed in a UV-ozone cleaner (Jelight 42-220) for 20 min. The electroluminescence devices were made as follows. First, a 100 nm layer of PEDOT:PSS (poly (3,4-ethylenedioxythiophene) : poly (styrenesulfonate), CLEVIO^{STM} PVP AI 4083, aqueous dispersion, 1.3–1.7% solid content, Heraeus) was spin-coated on the ITO glass substrate to improve the reproducibility of the devices and to prevent the formation of pinholes. Then, 80 nm transparent films of the complexes and BMIM-PF_6 in a 4 to 1 molar ratio were spin-coated from 20 $mgmL^{-1}$ acetonitrile solution at 1000 rpm for 20 s. The solutions were filtered using a 0.1 mm PTFE-filter and spin-coated on top of the PEDOT:PSS layer. The devices were transferred in an inert atmosphere glovebox (<0.1 ppm O_2 and H_2O, M. Braun). The Al electrode (70 nm) was thermally vapor deposited using a shadow mask under vacuum ($<10^{-6}$ mbar) using an Edwards Auto500 evaporator integrated in the glovebox. The area of the device was 6.5 mm^2. The devices were not encapsulated and were characterized inside the glovebox at room temperature. The device lifetime was measured by applying a pulsed current and monitoring the voltage and, simultaneously, the luminance by a True Colour Sensor MAZeT (MTCSiCT Sensor) with a Botest OLT OLED Lifetime-Test System. An Avantes luminance spectrometer was used to measure the electroluminescent spectra.

Results and discussion

Synthesis and characterization

The final products (see Figure 1) were fully characterized by FT IR spectroscopy, elemental analysis, and mono and bi-dimensional ^1H NMR spectroscopy. The complex $[Ir(F_2ppy)_2(ppz)][PF_6]$ was obtained in a lower yield than the analogous complex with the ppl ligand. This behavior is explained by the structure of the ppz ligand, which favours the simultaneous formation of both, mono and bi-metallic complexes. Therefore, to obtain the desired pure monometallic complex it was necessary to use a rigorous chromatography column procedure. For both complexes, the characterization by infrared spectroscopy showing the characteristic bands of PF_6^- counteranion around 843 and 557 cm^{-1}. The characterization by ^1H NMR spectroscopy show significant differences between

Table 2 Selected bond lengths and angles for Ir(III) complexes.

	$[Ir(F_2ppy)_2(ppl)]^+$	$[Ir(F_2ppy)_2(ppz)]^+$
Ir(1)-C(41)	1.997(4)	2.005(6)
Ir(1)-C(61)	2.008(4)	2.005(6)
Ir(1)-N(31)	2.047(3)	2.030(5)
Ir(1)-N(51)	2.047(3)	2.040(5)
Ir(1)-N(11)	2.136(3)	2.148(4)
Ir(1)-N(1)	2.146(3)	2.147(4)
C(41)-Ir(1)-N(31)	80.32(16)	79.80(2)
C(61)-Ir(1)-N(51)	80.06(15)	80.20(2)
N(11)-Ir(1)-N(1)	77.24(12)	77.02(16)

$[Ir(F_2ppy)_2(ppl)][PF_6]$ and $[Ir(F_2ppy)_2(ppz)][PF_6]$ complexes (see Figure S1 in the ESI†).The complex with ppl ligand present a high symmetry and a simple splitting pattern while that in the complex with ppz ligand, a loss of symmetry is observed by the splitting of the signals of each proton. In the case of the $[Ir(F_2ppy)_2(ppl)][PF_6]$ complex, the hydrogen signal of the pyrazine ring appears as a singlet at 9.36 ppm, while for $[Ir(F_2ppy)_2(ppz)][PF_6]$ complex two signals, at 9.41and ~ 8.68 ppm, are observed. The assignment of these protons required COSY experiments, which clearly indicated correlation with coupled protons. The characterization by X-ray diffraction confirms the successful synthesis of the complexes.

X-ray crystallography characterization

X-ray quality crystals of $[Ir(F_2ppy)_2(ppl)][PF_6]$ and $[Ir(F_2ppy)_2(ppz)][PF_6]$ were grown by diffusion of hexane in a CH_2Cl_2 solution of the complexes. The corresponding structures are depicted in Figure 2 and selected bond lengths and angles of the iridium coordination spheres are reported in Table 2.

Both complexes exhibit an expected slightly distorted octahedral geometry around the iridium center with the two pyridine rings in *trans*- position to each other. The chelating F_2ppy ligands are in a *trans*-disposition of the pyridine rings, similar to those observed in common heteroleptic Ir(III) complexes.[4,41-43] Geometrical parameters such as bond lengths and angles around the Ir atom are also in a similar range reported for other analogous complexes.[42,44,45]

The crystal structure of $[Ir(F_2ppy)_2(ppl)][PF_6]$ is stabilized by two stacking patterns: T-shaped, C4-H4···Cg2^i (Cg2: C12/C17) symmetry code i: 1-x, 2-y, 1-z, with H4···Cg2^i distance 2.504 Å, and offset face-to face Cg1-Cg1^i (Cg1: C1/C6) with centroid-centroid distance 3.650(3) Å complexes (see Fig. S2 in the ESI†).

Table 3 Electrochemical and photophysical properties of the cyclometalated Ir(III) complexes.

Complex	$E(Ir^{4+/3+})^a$/V	$E(red)^a$/V	λ_{abs}/nm^b (ε/M^{-1}cm^{-1})	λ_{em}/nm		Φ		τ/ns^b	$k_r(10^5)^d$	$k_{nr}(10^5)^d$
				Solution^b	Film^c	Solution^b	Film^c			
$[Ir(F_2ppy)_2(ppl)][PF_6]$	1.63	-1.22	358 (13235)	519	543	0.49	0.20	887	3.6	7.6
$[Ir(F_2ppy)_2(ppz)][PF_6]$	1.73	-0.93	360 (10112)	581	633	0.35	0.13	694	3.3	11.1

^{a}From CV measurement, $E(Ir^{4+/3+})$ = 1/2 (Epa + Epc); E(red) = Epc of reduction processes; acetonitrile/TBA-PF_6 0.1 M, vs. Ag/AgCl. ^{b}In acetonitrile at room temperature. ^{c}Thin solid film with (4:1, complex:BMIM-PF_6). ^{d}Calculated from solution data using $k_r = \Phi/\tau$ and $k_{nr} = 1/\tau - k_r$[49,50].

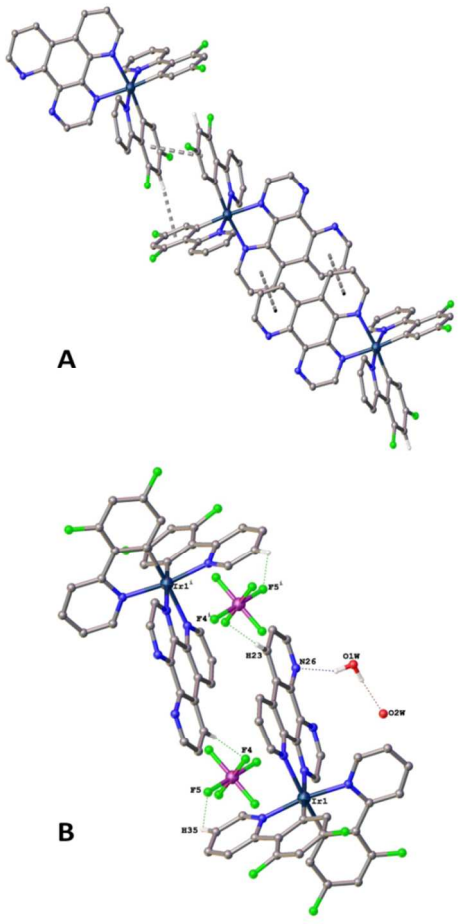

Fig. 3 π–π stacking interactions (A) and O–H···N, O–H···O and C–H···F hydrogen bonds (B) of $[Ir(F_2ppy)_2(ppz)][PF_6]$ complex. Hydrogen atoms were deleted to simplify.

T-shaped interaction generates centro symmetric dimmers reinforced by offset face-to face Cg1-Cg1^i interactions.

In the case of complex $[Ir(F_2ppy)_2(ppz)]^+$, was found that the crystal structure is stabilized by two stacking patterns: T-shaped, C4-H4···Cg2^i (Cg2: C12/C17) symmetry code i: 1-x, 2-y, 1-z, with H4···Cg2^i distance 2.504 Å, and off set face-to face Cg1-Cg1^i (Cg1:C1/C6) with centroid-centroid distance 3.650(3) Å. Showing distinct molecular interactions motifs, the complex with ppz ligand achieves a crystal structure stabilization by a network of O–H···N O–H···O and C–H···F hydrogen bonds and π–π stacking interactions [centroid–centroid =3.752(3) and 3.700(3) Å] between phenyls and pyrazines rings, as depicted in the Figure 3.

Electrochemical properties

Figure 4 shows the cyclic voltammograms (CV) recorded for $[Ir(F_2ppy)_2(ppl)][PF_6]$ and $[Ir(F_2ppy)_2(ppz)][PF_6]$ complexes in acetonitrile solution using Ag/AgCl as a reference electrode. The assignment of the redox processes was carried out by comparison

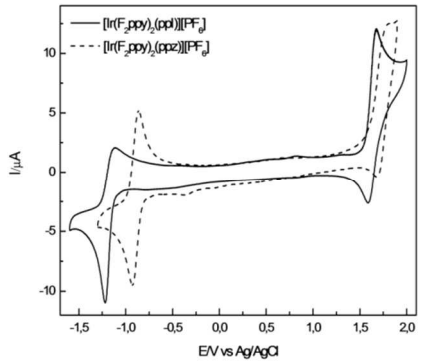

Fig. 4 Cyclic voltammetric profiles recorded in CH_3CN solution for$[Ir(F_2ppy)_2(ppl)][PF_6]$ (solid line) and $[Ir(F_2ppy)_2(ppz)][PF_6]$ (dashed line) complexes at 0.1 Vs^{-1}.

with electrochemical data reported for similar Ir(III) complexes.[46-48] The values of the oxidation/reduction potentials are given in Table 3.

The cyclic voltammograms of the complexes show a similar profile, where it is possible to observe a quasi-reversible redox process at 1.63 and 1.73 V, for complexes with ppl and ppz ligand, respectively, which can be attributed to the Ir(IV)/Ir(III) couple together with a contribution of the oxidation from the phenyl π orbital of the cyclometalated (C^N) ligands, as it has been described for these type of complexes.[5] Indeed our calculations show that the HOMO of both complexes appears composed by Ir_d (36%) and F_2ppy_π (64%) orbitals. In addition, the process observed at negative potentials, at -1.22 and -0.93 V for $[Ir(F_2ppy)_2(ppl)][PF_6]$ and $[Ir(F_2ppy)_2(ppz)][PF_6]$ complexes respectively, can be associated with the reduction of the N^N ligands[5] because of the LUMO was theoretically determined to be delocalized mainly on the phenanthrolic fragment with some contribution from pyrazinic ring; in the case of $[Ir(F_2ppy)_2(ppz)]^+$, the LUMO is delocalized in an aromatic zone (mixture of phenanthrolinic and pyrazinic regions) containing the three N atoms more closer bounded to the metal.

Note that the oxidation potentials values for both complexes are very similar due to the same nature of the species involved in this process. However, the first reduction process for the complex with ppz ligand is observed at less negative values compared with

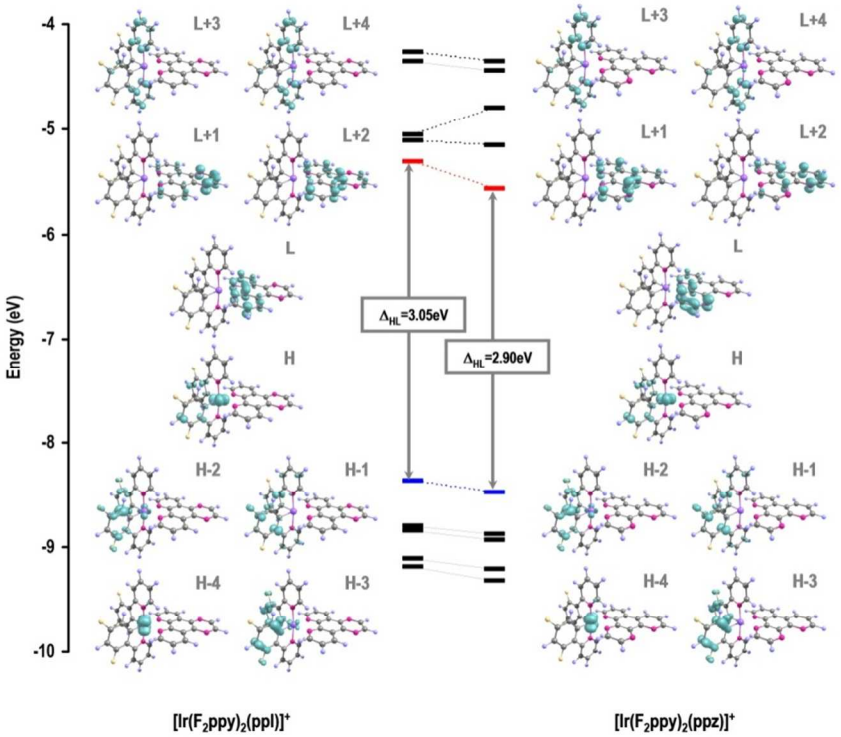

Fig. 5 Densities of frontier Kohn-Sham orbitals of $[Ir(F_2ppy)_2(ppl)]^+$ and $[Ir(F_2ppy)_2(ppz)]^+$ complexes. H: HOMO; L: LUMO; Δ_{HL}: H-L energy gap.

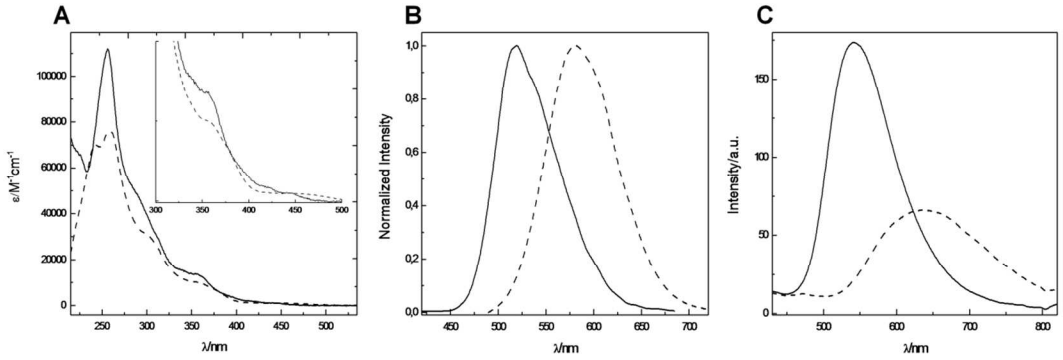

Fig. 6 Absorption (inset: 300-500 nm) (A) and emission (B) spectra in acetonitrile solution at room temperature. Emission spectra (C) of thin films containing 25% of $BMIMPF_6$.$[Ir(F_2ppy)_2(ppl)][PF_6]$ (solid line) and $[Ir(F_2ppy)_2(ppz)][PF_6]$(dashed line).

the complex with ppl ligand, suggesting that the electron acceptor performance of the ppz ligand causes a stabilization of the LUMO, which corroborates that the LUMO is usually located on the neutral (N^N) ancillary ligand.[51]Additionally, the tendency of the HOMO-LUMO gap can be estimated from the calculation of the energy between the oxidation potential and the reduction potential, obtaining 2.84 and 2.66 V for $[Ir(F_2ppy)_2(ppl)][PF_6]$ and $[Ir(F_2ppy)_2(ppz)][PF_6]$ complexes, respectively. Both the HOMO-LUMO gap trend and stabilization of the LUMO in the ppz based complex are in qualitatively agreement with the performed calculations as displayed in Figure 5.

Photophysical properties

The characteristic absorption pattern of the studied complexes in acetonitrile is evidenced in Figure 6A, and assignments were done from TD-DFT calculations (Table S2 in the supplemental material). At first glance, it is noted that there is not a meaningful difference in the UV-Vis spectra of $[Ir(F_2ppy)_2(ppl)]^+$ and $[Ir(F_2ppy)_2(ppz)]^+$. The absorption bands in the ultra-violet region between 250 and 290 nm are ascribed to spin allowed ligand-centered ^{1}(LC) ($\pi\rightarrow\pi^*$) transitions on the ancillary ligand (ppl and ppz). These bands appear theoretically with high oscillator strengths at 262 and 263 nm for the $[Ir(F_2ppy)_2(ppl)]^+$ complex, and at 277 nm for $[Ir(F_2ppy)_2(ppz)]^+$, in good agreement with the experimental absorption spectrum.

Focusing in the weak absorption bands between 350 and 410 nm, these are assigned to a mixture of ^{1}MLCT (metal-to-ligand charge

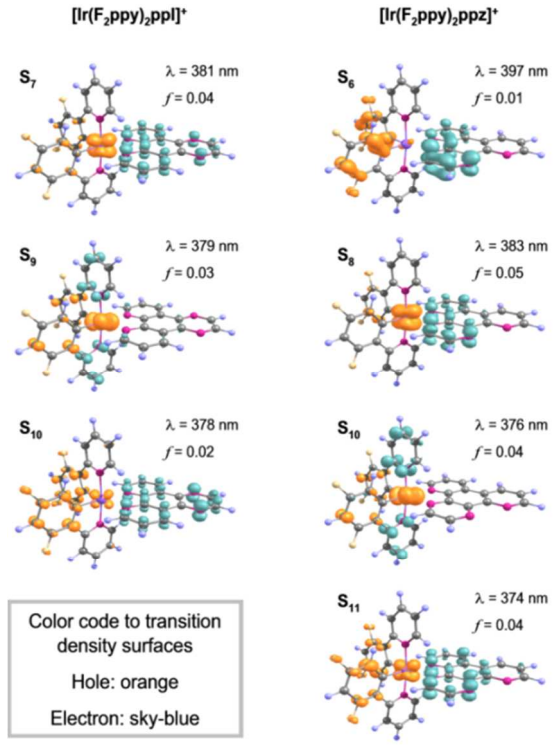

Fig. 7 Transition density surfaces depicting the hole-electron distributions of singlet (S_i) allowed transitions between 360 to 400 nm of $[Ir(F_2ppy)_2(ppl)]^+$ and $[Ir(F_2ppy)_2(ppl)]^+$. λ: wavelength; f: oscillator strength. See supplementary information to details about electronic transitions.

transfer) and ^{1}LLCT transitions (ligand to ligand charge transfer) as in related Ir(III) complexes[5], involving electron promotion from metal and F_2ppy_π orbitals toward π* orbitals of ppl or ppz (Figure 7); specifically, the excited states are involving frontier orbitals ranging from HOMO-5 until LUMO+3. In particular, these bands appear experimentally centered at 358 and 360 nm, for the complexes with the ppl and the ppz ligand, respectively. In the case of the $[Ir(F_2ppy)_2(ppz)][PF_6]$ complex, a slightly red shift of this band is observed in comparison with the spectrum of the $[Ir(F_2ppy)_2(ppl)][PF_6]$ complex, which can be related to the electron-withdrawing character of the ppz ligand in comparison with ppl ligand, as obtained from electrochemical measures. In addition TD-DFT calculations show that ^{1}MLCT and ^{1}ILCT (intraligand charge transfer) transitions take place in this region of the UV-Vis spectra, where an electron is promoted to the F_2ppy ligand.

Moreover, in these type of complexes, it is also possible to observe bands above 450 nm due to direct spin-forbidden population of the triplet excited states, which are enabled by the high spin-orbit coupling of the iridium metal.[52] These type of bands are not clearly observed in the spectra of the complexes in study due to the low molar extinction coefficients (see inset Fig. 6A). In addition, TD-DFT calculation shows that HOMO-LUMO transitions are not allowed in the present compounds.

The emission spectra of the complexes registered at room temperature from deaerated acetonitrile solution, and excited in the ^{1}MLCT band, are displayed in Figure 6B. The emission band of $[Ir(F_2ppy)_2(ppz)][PF_6]$ complex is shifted by 62 nm towards lower energies compared to $[Ir(F_2ppy)_2(ppl)][PF_6]$ complex (see Table 3). The $[Ir(F_2ppy)_2(ppl)][PF_6]$ complex exhibits a photoluminescence quantum yield 1.39 times higher than $[Ir(F_2ppy)_2(ppz)][PF_6]$ which is evidently associated with the lower emission intensity observed for the last one. The behavior of these complexes show the same tendency as that of the analogous complexes containing Ru(II) as transition metal, namely, the $[Ru(bpy)_2(ppl)][PF_6]_2$ and $[Ru(bpy)_2(ppz)][PF_6]_2$ complexes.[53] Consequently, in the complexes with ppz ligand the delocalization of the electronic density shifted the emission to lower energies, causing an increment of the k_{nr} constant value (the k_{nr} of $[Ir(F_2ppy)_2(ppz)][PF_6]$ being 1.5 times higher than $[Ir(F_2ppy)_2(ppl)][PF_6]$). This behavior is associated with the lower value registered for the excited-state lifetime for $[Ir(F_2ppy)_2(ppz)][PF_6]$ complex in comparison with the value of the $[Ir(F_2ppy)_2(ppl)][PF_6]$ complex, according to the prediction of the energy gap law.[54]

The emission spectra of the complexes in thin solid film were also obtained by spin coating an acetonitrile solution of each complex mixed with the ionic liquid BMIM-PF_6 in a 4:1 molar ratio (see Figure 6C). The inclusion of an ionic liquid allows to obtain the emission performance of the complexes in a similar situation to the LEC device configurations. Basically, the ionic liquid is incorporated to diminish the turn on time of the LEC devices, as described in the literature.[55] Compared with their emission spectra in solutions, the emission spectra of the complexes $[Ir(F_2ppy)_2(ppl)][PF_6]$ and $[Ir(F_2ppy)_2(ppz)][PF_6]$ in thin solid films are red-shifted and show long tails. As shown in Table 3, the Φ in thin films tend to decrease in comparison with the Φ in solution. This behavior is related to strong intermolecular interactions due to the close packaging of the luminescent molecules in the thin solid films, which promote the auto-quenching processes.[56] The red-shift is very pronounced in the case of the complex with ppz ligand. A possible explanation of this conduct could be the increment of the inter- and intramolecular interactions in this complex, as described in the X-ray section.

The tendency of the higher Φ measured for the $[Ir(F_2ppy)_2(ppl)][PF_6]$ complex is in line with the performance observed in solution. The lower Φ observed for $[Ir(F_2ppy)_2(ppz)][PF_6]$ in solid is concordant with the lower energy of the emitting triplet state (energy gap law). The description developed for photophysical properties of the Ir(III) complexes studied is in good agreement with the data of the literature of these kind of complexes.[57]

In order to characterize the emissive state of interest for LEC applications, firstly the lowest spin forbidden transitions to the excited states due to vertical transitions from the S_0 ground state were analysed. The first triplet (T_1) state appears at 527 and 572 nm for $[Ir(F_2ppy)_2(ppl)]^+$ and $[Ir(F_2ppy)_2(ppz)]^+$ respectively, which are close to the experimental emission. The T_1 state is a mixture of ^{3}MLCT and ^{3}LLCT transitions involving the HOMO and LUMO orbitals. In addition, the T_2 and T_3 states appear with a shift of at least 71 nm from the T_1 state, therefore, emission would occur only from the T_1 state. These transitions are shown in Table S3 in the ESI†. The adiabatic emission energies were calculated in gas phase to best comparison with the experimental measurements in solid state. In the relaxed T_1 states,

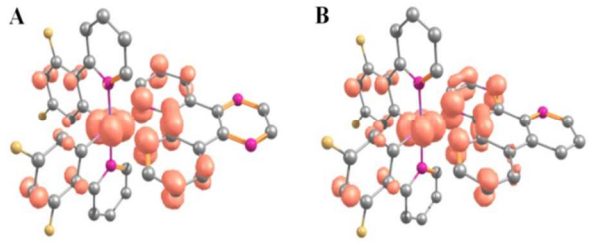

Fig. 8 Isosurfaces of spin density distribution in the relaxed T_1 state of $[Ir(F_2ppy)_2(ppl)]^+$ (A) and $[Ir(F_2ppy)_2(ppz)]^+$ (B). For simplicity hydrogen atoms were not drawn.

phosphorescent emissions energies of both complexes appear ~30 nm red shifted from the first singlet-triplet excitation. The emission energies were estimated at 2.23 eV and 2.05 eV for $[Ir(F_2ppy)_2(ppl)]^+$ and $[Ir(F_2ppy)_2(ppz)]^+$, respectively, in agreement with those obtained from solid state measurements with values of 2.28 and 2.05 eV, respectively. In addition, emission at low energies observed for $[Ir(F_2ppy)_2(ppz)]^+$ respecting $[Ir(F_2ppy)_2(ppl)]^+$ are only due to the more stabilized nature of the frontier orbitals in the ppz based complex. In summary, the calculations shows that emissions of the complexes occurs only from T_1 state, different of reported Ir(III) complexes where emission occurs by mixture of the first four low-lying triplets state, causing occurrence of a red-shifted emission.[58] Firstly, mixture of ^{3}MLCT and ^{3}LLCT transitions for the T_1 state was confirmed from its spin density distribution (Figure 8); for $[Ir(F_2ppy)_2(ppl)]^+$, the spin densities by fragment were 0.52 (Ir), 0.40 (F_2ppy) and 1.08 (ppl); while for $[Ir(F_2ppy)_{2(}ppz)]^+$ were 0.50 (Ir), 0.43 (F_2ppy) and 1.07 (ppz).

Electroluminescent properties

LEC devices were fabricated by spin coating the complexes on a suitable hole injection layer previously deposited on a patterned indium tin oxide (ITO)-covered glass substrate. Prior to the deposition of the emitting layer, a 100 nm layer of poly-(3,4-ethylenedioxythiophene):poly-(styrenesulfonate) (PEDOT:PSS), as the hole injection layer, was deposited onto the ITO anode with the goal of increasing the yield and reproducibility of the working devices. The 80 nm emitting layer was prepared by dissolving the corresponding complex and the ionic liquid 1-butyl-3-methylimidazolium hexafluorophosphate (BMIM-PF_6) at a molar ratio of 4 to 1 in acetonitrile. The ionic liquid was used to enhance the ionic conductivity of the active layer and to reduce the turn-on time of the devices.[59] A 70 nm aluminum cathode was thermally evaporated on top of the device under high vacuum. The LECs were operated under inert conditions applying pulsed current methods with an average current density of 100 Am^{-2} using a duty cycle of 50%[60] and monitoring the voltage and the luminance, simultaneously.

For the ITO/PEDOT:PSS/Ir complex:BMIM-PF_6 (4:1)/Al devices, the light emission was observed for the LEC employing $[Ir(F_2ppy)_2(ppl)][PF_6]$ complex (see Fig. 9). The LEC employing the $[Ir(F_2ppy)_2(ppz)][PF_6]$ complex practically did not show light emission. This behavior is in agreement with the luminescent studies in solution and in the solid film where the low quantum yield for the complex with the ppz ligand indicates that the more

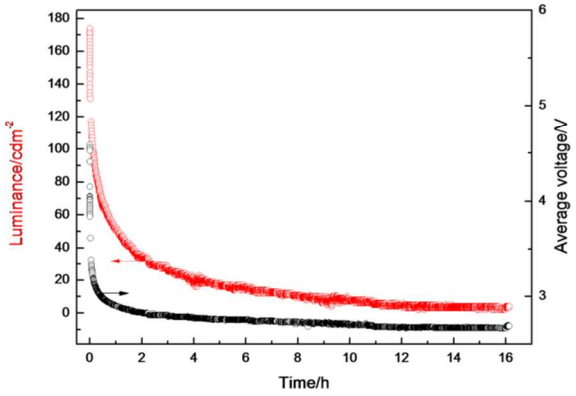

Fig. 9 Luminance (red) and average voltage (black) for LEC device characterization with an average current density of 100 Am^{-2} using a duty cycle of 50%.

Table 4 Performance of $[Ir(F_2ppy)_2(ppl)][PF_6]$ LEC devices.

t_{on}/h	0.03
Luminance/cdm^{-2}	177
$t_{1/2}$/h	0.22
Efficacy/cdA^{-1}	1.57
Power efficiency/lmW^{-1}	0.61
EQE	0.46

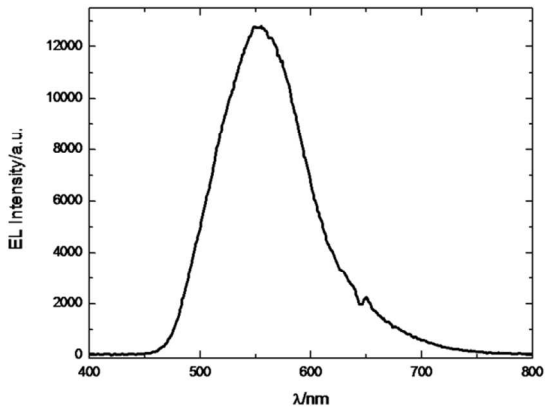

Fig. 10 Normalized electroluminescent spectrum of LEC device with an average current density of 100 Am^{-2} using a duty cycle of 50%.

electron withdrawing character of the ppz ligand generates the stabilization of the LUMO. In addition, as is inferred from the crystal structure, the inter- and intramolecular interactions present in the complex with ppz ligand are greater than the ones of the complex with ppl, therefore favouring the non-radiative decay, and causing a negative effect on the LEC performance.

The LEC employing the $[Ir(F_2ppy)_2(ppl)][PF_6]$ complex displayed a rapid increase in the luminance for which a maximum was reached after approximately 1.6 minutes of device operation. The values of the external quantum efficiency (EQE) for this LEC are shown in Table 4.

Fig. 10 displays the electroluminescent spectra of $[Ir(F_2ppy)_2(ppl)][PF_6]$ LEC that exhibits green electroluminescence with the maxima located at about 554 nm. This spectrum is red shifted with respect to the emission spectra in thin solid film. Hence, this red-shift is related to a change in the film composition rather than due to the manner of excitation

used. The CIE (International Commission on Illumination) coordinates determined from electroluminescent spectra are (0.39, 0.56).

Compared to related complexes,[61] using similar conditions (complex:ionic liquid, 4:1) but applying 3 V instead of pulsed current of 100 Am^{-2}, the luminance maxima and turn on times of the $[Ir(F_2ppy)_2(ppl)][PF_6]$ complex are better, showing its promise as luminescent material for possible LEC applications.

Conclusions

The effect of the position of the phenanthrolinic nitrogens in the structure of the ancillary ligand in two cyclometalated Ir(III) complexes was evaluated. In particular, the complexes of the kind $[Ir(F_2ppy)_2(N^N)][PF_6]$, where N^N are pyrazino [2,3-f][1,10]-phenanthroline (ppl) and pyrazino[2,3-f][4,7]phenanthroline (ppz), were analyzed in terms of their electrochemical and photophysical properties in the framework of experimental analysis and quantum chemical calculations. According to the emission spectra, registered both in solution and in thin solid film, it was found that the $[Ir(F_2ppy)_2(ppl)][PF_6]$ complex has higher quantum yield and a longer excited state lifetime compared to $[Ir(F_2ppy)_2(ppz)][PF_6]$.The behavior shown by the ppz based complex is explained by the electron withdrawing character of this ligand, causing the stabilization of the LUMO, promoting a decrease of the HOMO-LUMO gap and favouring the non-radiative decay in concordance with the energy gap law. Moreover, both complexes were evaluated for LEC applications, obtaining light emission only in the case of $[Ir(F_2ppy)_2(ppl)][PF_6]$. In the case of the $[Ir(F_2ppy)_2(ppz)][PF_6]$ complex, the absence of luminance was ascribed to both LUMO stabilization and enhanced intermolecular interactions which lead to the non-radiative decay. Consequently, these synergetic effects contribute to the poor LEC performance.

The LEC with the complex with ppl ligand stands out by a very short turn on time, which is an important characteristic to consider when choosing a luminescent material for LEC fabrication.

Acknowledgements

This work was financially supported by FONDECYT Chile Projects N° 1110991 and Nº 11130221, the Generalitat Valenciana (Prometeo/2012/053) and the USM-Projects Nº 131439 and Nº131319. I.G. acknowledges a doctoral fellowship of CONICYT. D.C-A thanks to ICM grant N°120082. M.S thanks ajeya-ameya systems for computational facilities. The authors acknowledge Dr. M. Isaacs, Dr. M. Soto-Arriaza and F. Castillo of Pontificia Universidad Católica de Chile for the help on the experimental measurements and discussions.

Notes and references

[a] *Departamento de Química Inorgánica, Facultad de Química, Pontificia Universidad Católica de Chile, Av. Vicuña Mackenna 4860, Macul, Santiago, Chile. E-mail:* ilgonzalez@uc.cl

[b] *Departamento de Química, Universidad Técnica Federico Santa María, Av. España 1680, Valparaíso, Chile. E-mail:* paulina.dreyse@usm.cl

[c] *Nucleus Millennium Chemical Processes and Catalysis, Laboratorio de Química Teórica Computacional(QTC), Departamento de Química-Teórica, Facultad de Química, Pontificia Universidad Católica de Chile, Av. Vicuña Mackenna 4860, Macul, Santiago, Chile. E-mail:* dcortesr@uc.cl

[d] *Theoretical Chemistry Section, Bhabha Atomic Research Centre, Mumbai – 400 085, India, E-mail:* smahesh@barc.gov.in

[e] *Departamento de Química, Universidad de Antofagasta, Av. Angamos 601, Antofagasta, Chile.*

[f] *Instituto de Ciencia Molecular, Universidad de Valencia, 46980 Paterna, Spain. E-mail:* henk.bolink@uv.es

†Electronic Supplementary Information (ESI) available: Fig. S1 ^{1}H-NMR spectrum. Fig. S2 π–π stacking interactions of $[Ir(F_2ppy)_2(ppl)][PF_6]$ complex. Fig. S3 Ground state optimized structures. Fig. S4 First triplet state optimized structures. Table S1, Optimized structural parameters. Table S2, Excitation energies of singlet excited states. Table S3, Excitation energies of triplet states. CCDC 1044762 and 1027525. For ESI and crystallographic data see DOI: 10.1039/b000000x/

1. Z. Ning, Q. Zhang, W. Wua, H. Tian, *J. Organomet. Chem.,* 2009, **694**, 2705.
2. E. Baranoff, J-H. Yum, M. Gräetzel, Md. K. Nazeeruddin, J. *Organomet. Chem.,* 2009, **694**, 2661.
3. A. Valore, A. Colombo, C. Dragonetti, S. Righetto, D. Roberto, R. Ugo, F. De Angelis,S. Fantacci, *Chem. Commun.,* 2010, **46**, 2414.
4. S. Lamansky, P. Djurovich, D. Murphy, F. Abdel-Razzaq, H-E. Lee, C. Adachi, P. E. Burrows, S. R. Forrest, M. E. Thompson, *J. Am. Chem. Soc.,* 2001, **123**, 4304.
5. R. D. Costa, E. Ortí, H. J. Bolink, F. Monti, G. Accorsi, N. Armaroli, *Angew. Chem. Int. Ed.,* 2012, **51**, 8178.
6. M. S. Lowry, S. Bernhard, *Chem. Eur. J.*, 2006, **12**, 7970.
7. L. He, J. Qiao, I. Duan, G. Dong, D. Zhang, L. Wang, Y. Qiu, *Adv. Funct. Mater.,* 2009, **19**, 2950.
8. Y. You, Y. Park, *J. Am. Chem. Soc.,* 2005, **127**, 12438.
9. J. D. Slinker, J. Rivnay, J. S. Moskowitz, J. B. Parker, S. Bernhard, H. D. Abruña, G. G. Malliaras, *J. Mater. Chem.,* 2007, **17**, 2976.
10. T. Hu, L. He, L. Duan, Y. Qiu, *J. Mater. Chem.,* 2012, **22**, 4206.
11. H. J. Bolink, L. Cappelli, E. Coronado, P. Gaviña, *Inorg. Chem.,* 2005, **44**, 5966.
12. P. Matyba, K. Maturova, M. Kemerink, N. D. Robinson, L. Edman, *Nat. Mater.,* 2009, **8**, 672.
13. K. M. Maness, R. H. Terrill, T. J. Meyer, R. W. Murray, R. M. Wightman, *J. Am. Chem. Soc.,* 1996, **118**, 10609.
14. Q. Pei, G. Yu, C. Zhang, Y. Yang, A. J. Heeger, *Science*, 1995, **269**, 1086.
15. C. Ulbricht, B. Beyer, C. Friebe, A. Winter, U. S. Schubert, *Adv. Mater.,* 2009, **21**, 4418.
16. F. De Angelis, S. Fantacci, N. Evans, C. Klein, S. M. Zakeeruddin, J. E. Moser, K. Kalyanasundaram, H. J. Bolink, M. Grätzel, M. K. Nazeeruddin, *Inorg. Chem.,* 2007, **46**, 5989.
17. L. He, J. Qiao, I. Duan, G. Dong, D. Zhang, L. Wang, Y. Qiu, *Adv. Funct. Mater.,* 2009, **19**, 2950.
18. J. G. Collins, A. D. Sleeman, J. R. Aldrich-Wright, I. Greguric, T. Hambley, *Inorg. Chem.,* 1998, **37**, 3133.
19. A. Francois, R. Díaz, A. Ramírez, B. Loeb, M. Barrera, I. Crivelli, *Polyhedron,* 2013, **52**, 62.
20. P. Schmidt, J. Druey, *Helv. Chim. Acta,* 1957, **42**, 350.
21. C. Abeywickrama, A. D. Baker. *J. Org. Chem.,* 2004, **69**, 7741.
22. M. Lowry, J. Goldsmith, J. D. Slinker, R. Rohl, R. Pasca, G. Malliaras, S. Bernhard, *Chem. Mater.,* 2005, **17**, 5712.
23. G. Ge, X. Yu, H. Guo, F. Wang, D. Zou, *Synth. Met.,* 2009, **159**, 1178.
24. Stoe&Cie (2001). X-AREA and X-RED. Stoe&Cie, Darmstadt, Germany.
25. G. M. Sheldrick, *ActaCrystallogr. Sect. A: Found. Crystallogr.,* 2008, **64**, 112.
26. H. Ishida, S. Tobita, Y. Hasegawa, R. Katoh, K. Nozaki, *Coord. Chem. Rev.* 2010, **254**, 2449–2458.
27. R. Spencer, G. Weber, *Ann. NY Acad. Sci.,* 1969, **158**, 331.
28. R. Spencer, G. Weber G, *J. Chem. Phys.,* 1970, **52**, 1654.
29. E. Gratton, D. Jameson, R. D. Hall, *Ann. Rev. Biophys. Bioeng.,* 1984, **13**, 105.
30. J. R. Alcala, E. Gratton, F. G. Prendergast, *Biophys. J.,* 1987, **51**, 587.

31. D. Jameson, E. Gratton, R. D. Hall, *Appl. Spectrosc. Rev.,* 1984, **20**, 55.
32. S. Panozzo, M. Armand, O. Stéphan, *Appl. Phys. Lett.,* 2002, **80**, 679.
33. A. D. Becke, *J. Chem. Phys.*, 1993, **98**, 5648.
34. A. Schäfer, H. Horn, R. Ahlrichs, *J. Chem. Phys.,* 1992, **97**, 2571.
35. D. Andrae, U. Häußermann, M. Dolg, H. Soll, H. Preuß, *Theor. Chim. Acta,* 1990, **77**, 123.
36. F. Weigend, R. Ahlrichs, *Phys. Chem. Chem. Phys.*, 2005, **7**, 3297.
37. S. Hirata, M. Head-Gordon, *Chem. Phys. Lett.,* 1999, **314**, 291.
38. F. Neese, *Wires: Comp. Mol. Sci.,* 2012, **2**, 73.
39. A. Hellweg, C. Hättig, S. Höfener, *Theor. Chem. Acc.,* 2007, **117**, 587.
40. E. D. Glendening, C. R. Landis, F. Weinhold, *J. Comp. Chem.,* 2013, **34**, 1429.
41. E. Baranoff, I. Jung, R. Scopelliti, E. Solari, M. Grätzel, M. K. Nazeeruddin, *Dalton Trans.,* 2011, **40**, 6860.
42. S. Lamansky, P. Djurovich, D. Murphy, F. Abdel-Razzaq, R. Kwong, I. Tsyba, M. Bortz, B. Mui, R. Bau, M. E. Thompson, *Inorg. Chem.,* 2001, **40**, 1704.
43. R. S. Vadavi, H. Kim, K. M. Lee, T. Kim, J. Lee, Y. S. Lee, M. H. Lee, *Organometallics,* 2012, **31**, 31.
44. R. M. Edkins, A. Wriglesworth, K. Fucke, S. L. Bettington, A. Beeby, *Dalton Trans.,* 2011, **40**, 9672.
45. E. Baranoff, B. F. E. Curchod, J. Frey, R. Scopelliti, F. Kessler, I. Tavernelli, U. Rothlisberger, M. Grätzel, M. K. Nazeeruddin, *Inorg. Chem.,* 2012, **51**, 215.
46. F. Neve, A. Crispini, S. Campagna, S. Serroni, *Inorg. Chem.,*1999, **38**, 2250.
47. Y. Ohsawa, S. Sprouse, K. A. King, M. K. DeArmond, K. W. Hanck, R. J. Watts, *J. Phys. Chem.,*1987, **91**, 1047.
48. P. Didier, I. Ortmans, A. Kirsch-De Mesmaeker, R. J. Watts, *Inorg. Chem.,* 1993, **32**, 5239.
49. C. Bronner, M. Veiga, A. Guenet, L. De Cola, M. W. Hosseini, C. A. Strassert, S. A. Baudron, *Chem. Eur. J.,* 2012, **18**, 4041.
50. F. Kessler, R. D. Costa, D. Di Censo, R. Scopelliti, E. Ortí, H. J. Bolink, S. Meier, W. Sarfert, M. Gräetzel, Md. K. Nazeeruddin, E. Baranoff, *Dalton Trans.,* 2012, **41**, 180.
51. R. D. Costa, E. Ortí, H. J. Bolink, S. Graber, C. E. Housecroft, E. C. Constable, *Adv. Funct. Mater.,* 2010, **20**, 1511.
52. M. Montalti, A. Credi, L. Prodi, M. T. Gandolfi, *Handbook of Photochemistry*, 3rd ed., Taylor and Francis, Boca Raton, FL, 2006.
53. M. Arias, J. Concepción, I. Crivelli, A. Delgadillo, R. Díaz, A. Francois, F. Gajardo, R. López, A. M. Leiva, B. Loeb, *Chem. Phys.,* 2006, **326**, 54.
54. G. F. Strouse, J. R. Schoonover, R. Duesing, S. Boyde, W. E. Jones, Jr., T. J. Meyer, *Inorg. Chem.,* 1995, **34**, 413.
55. R. D. Costa, A. Pertegás, E. Ortí, H. J. Bolink, *Chem. Mater.,* 2010, **22**, 1288.
56. L. He, L. Duan, J. Qiao, R. Wang, P. Wei, L. Wang, Y. Qiu, *Adv. Funct. Mater.,* 2008, **18**, 2123.
57. S. Campagna, F. Puntoriero, F. Nastasi, G. Bergamini, V. Balzani, *Photochemistry and Photophysics of Coordination Compounds I*; Springer: 2007, p 117.
58. H. Bolink, L. Cappelli, S. Cheylan, E. Coronado, R. D. Costa, N. Lardiés, M. K. Nazeeruddin, E. Ortí, J. Mater. Chem., 2007,**17**, 5032.
59. S. T. Parker, J. D. Slinker, M. S. Lowry, M. P. Cox, S. Bernhard, G. G. Malliaras, *Chem. Mater.,* 2005, **17**, 3187.
60. D. Tordera, S. Meier, M. Lenes, R. D. Costa, E. Ortí, W. Sarfert, H. J. Bolink, *Adv. Mater.,* 2012, **24**, 897.
61. R. D. Costa, E. Ortí, H. J. Bolink, S. Graber, S. Schaffner, M. Neuburger, C. E. Housecroft, E. C. Constable, *Adv. Funct. Mater.*, 2009, **19**, 3456.